Article

Haze Occurrence Caused by High Gas-to-Particle Conversion in Moisture Air under Low Pollutant Emission in a Megacity of China

Qingxia Ma [1,2], Weisi Wang [3], Dexin Liu [1], Rongke Zhao [4], Jingqi Zhao [1], Wanlong Li [1], Yanfang Pan [1,*] and Daizhou Zhang [5,*]

1 Key Laboratory of Geospatial Technology for the Middle and Lower Yellow River Regions, Ministry of Education, College of Geography and Environmental Science, Henan University, Kaifeng 475004, China; mqx@henu.edu.cn (Q.M.); dxliu@vip.henu.edu.cn (D.L.); zhaojingqi@henu.edu.cn (J.Z.); liwanlong@henu.edu.cn (W.L.)
2 Henan Key Laboratory of Integrated Air Pollution Control and Ecological Security, Kaifeng 475004, China
3 Henan Ecological and Environmental Monitoring Center, Zhengzhou 450007, China; cameraart@126.com
4 Henan Kaifeng College of Science Technology and Communication, Kaifeng 475004, China; zrk_heart@163.com
5 Faculty of Environmental and Symbiotic Sciences, Prefectural University of Kumamoto, Kumamoto 862-8502, Japan
* Correspondence: panyanfang@henu.edu.cn (Y.P.); dzzhang@pu-kumamoto.ac.jp (D.Z.)

Abstract: Haze occurred in Zhengzhou, a megacity in the northern China, with the $PM_{2.5}$ as high as 254 $\mu g\ m^{-3}$ on 25 December 2019, despite the emergency response measure of restriction on the emission of anthropogenic pollutants which was implemented on December 19 for suppressing local air pollution. Air pollutant concentrations, chemical compositions, and the origins of particulate matter with aerodynamic diameter smaller than 2.5 μm ($PM_{2.5}$) between 5–26 December were investigated to explore the reasons for the haze occurrence. Results show that the haze was caused by efficient SO_2-to-suflate and NO_x-to-nitrate conversions under high relative humidity (RH) condition. In comparison with the period before the restriction (5–18 December) when the $PM_{2.5}$ was low, the concentration of $PM_{2.5}$ during the haze (19–26 December) was 173 $\mu g\ m^{-3}$ on average with 51% contributed by sulfate (31 $\mu g\ m^{-3}$) and nitrate (57 $\mu g\ m^{-3}$). The conversions of SO_2-to-sulfate and NO_x-to-nitrate efficiently produced sulfate and nitrate although the concentration of the two precursor gases SO_2 and NO_x was low. The high RH, which was more than 70% and the consequence of artificial water-vapor spreading in the urban air for reducing air pollutants, was the key factor causing the conversion rates to be enlarged in the constriction period. In addition, the last 48 h movement of the air parcels on 19–26 December was stagnant, and the air mass was from surrounding areas within 200 km, indicating weather conditions favoring the accumulation of locally-originated pollutants. Although emergency response measures were implemented, high gas-to-particle conversions in stagnant and moisture circumstances can still cause severe haze in urban air. Since the artificial water-vapor spreading in the urban air was one of the reasons for the high RH, it is likely that the spreading had unexpected side effects in some certain circumstances and needs to be taken into consideration in future studies.

Keywords: haze; gas-to-particle conversion; high RH; urban pollution; emission restriction

1. Introduction

Severe haze with high $PM_{2.5}$ concentration frequently occurs in the North China Plain (NCP) of China, imposing serious burden to the environment and threats to public health [1–3]. In order to suppress the heavy air pollution, the Chinese government has taken a series of control measures, including cutting down pollutant emissions, limiting car-use, constructing clean-coal power plants, prohibiting open burning of crop residues

during harvest seasons, etc. [4,5]. As a result, the annual mean $PM_{2.5}$ concentration significantly reduced nationwide in the past several years [6]. Yet, $PM_{2.5}$ concentration in many megacities of the NCP became high sometimes [7].

Previous studies have shown that the formation of secondary inorganic aerosols (SIAs, the sum of sulfate (SO_4^{2-}), nitrate (NO_3^-), and ammonium (NH_4^+)) was one of the major reasons causing the haze pollution with its 40–70% contribution to $PM_{2.5}$ in the NCP on an average basis [8,9]. The nonlinear relation between the decreases of sulfate and nitrate and their precursors has not been well understood, although the complex formation and atmospheric transformation processes are likely mediated by meteorological conditions [10,11]. For example, high relative humidity (RH > 60%) facilitates SIA formation via heterogeneous reactions and aqueous-phase reactions [12,13]. O_3 oxidation is a pathway for nitrate and sulfate formation under alkaline conditions [14,15]. Moisture conditions favored the formation of SIAs via heterogeneous reactions, and dry conditions inhibited gas-to-particle partitioning [8,16,17].

The current pollution control in China enabled substantial reduction of air pollutants from transportation, industrial, and human activities. However, haze still occurred sometimes in winter, indicating that the reduction did not stop the formation of haze [18–20]. The nonlinear relationships between the reductions of particulate matter (PM) and their precursors, unfavorable meteorological conditions, and enhanced secondary production were reported as the causes for the haze [10,21–25].

Zhengzhou is a megacity, with a population of approximately 12.6 million and land area of about 7567 km^2, which has high coal consumption, large transportation systems, and concentrative industries [26,27]. The city, located in the southern part of the NCP, is surrounded by other densely populated and industrialized cities. Serious air pollution and low visibility frequently occurred in the city (Figure 1, [22,28–30]). Due to the variety of energy structures and economy levels from city to city in China, one-city-one air pollution control-policy is urgently required [10,23].
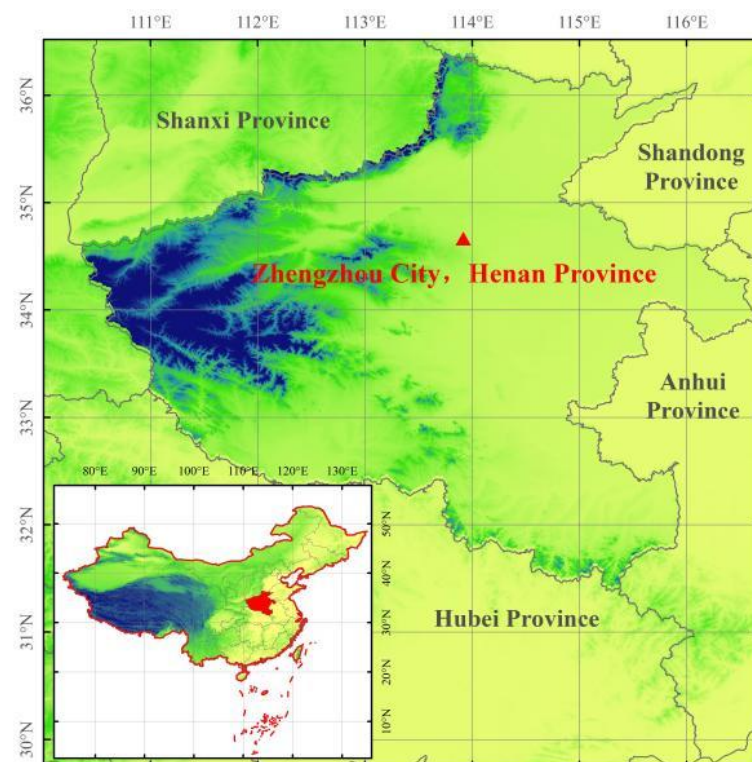

Figure 1. Location of the site (Zhengzhou) and topography in China.

Int. J. Environ. Res. Public Health **2022**, *19*, 6405

3 of 13

Zhengzhou implemented emergency response measures, such as shutting down and restricting industrial activities, prohibiting open burning, reducing heavy vehicles on roads, and spreading water vapor on public roads since 19 December 2019 to suppress the occurrence of haze [31]. However, a severe haze occurred between 19–26 December. The purpose of this study is to explore the reasons for the haze occurrence with the routine data from an urban monitoring site on air pollutant concentration, chemical composition, and the modelled origins of the $PM_{2.5}$ under control measure conditions and non-control measures conditions.

2. Materials and Methods

2.1. Observation Site and Instruments

The concentrations of air pollutants including $PM_{2.5}$, PM_{10}, O_3, SO_2, NO_x, and CO and meteorological conditions including pressure, temperature, RH, wind speed, wind direction, and precipitation are routinely measured at the environment monitoring supersite of Henan province in Zhengzhou (34.76° N, 113.70° E; Figure 1). The instruments are a series of pollutant detectors (5030, 5014i, 49I, 42I, 43I, 48I; Thermo Fisher Scientific, Waltham, MA, USA) and a weather station (Vantage VUE, Davis Instruments, Inc., Hayward, CA, USA) at a time resolution of 5 min. One-hour average of the air pollutants and weather conditions was applied.

The hourly mass concentrations of major water-soluble inorganic ions, including NH_4^+, Na^+, K^+, Ca^{2+}, Mg^{2+}, SO_4^{2-}, NO_3^-, and Cl^- in aerosols, were measured by an online analyzer for Monitoring of AeRosols and GAses (MARGA, model ADI 2080 Applikon Analytical B. V. Corp., Delft, The Netherlands) at a flow rate of 16.7 L min^{-1} [32,33]. A thermo-optical OC/EC analyzer (Model RT-4, Sunset Lab., Los Angeles, CA, USA) measured organic carbon (OC) and elemental carbon (EC) in aerosol particles. Elements in $PM_{2.5}$, including K, Ca, Pb, Se, Cr, Zn, Cu Ni, Fe, Mn, Ti, V, Ba, As, Co, Mo, Sc, Br, Si, and Al, were quantified by an online analyzer for monitoring (AMMS-100, Focused Photonics Inc., Hangzhou, China). The formulas of major components in the $PM_{2.5}$ and the conversion rates of SO_2 to sulfate (SOR) and NO_x to nitrate (NOR) are listed in Table 1.

Table 1. Formulas and references of main components in $PM_{2.5}$.

Components or Their Conversions	Formulas	References
Secondary inorganic aerosols (SIAs)	$SO_4^{2-} + NO_3^- + NH_4^+$	[6,34]
Organic matter (OM)	$1.6 \times OC$	[7,35]
Mineral	$2.20\ Al + 2.49\ Si + 1.63\ Ca + 2.42\ Fe + 1.94\ Ti$	[36,37]
Sea salt	$Mg^{2+} + Na^+ + F^- + Cl^-$	[38]
K salt	K^+	[39]
SOR	$[SO_4^{2-}]/([SO_4^{2-}] + [SO_2])$ molar concentration	[40]
NOR	$[NO_3^-]/([NO_3^-] + [NO] + [NO_2])$	[41]

Where [x] is the molar concentration of x species.

In this study, the observational data between 5–26 December of 2019 were utilized. Three haze events in the observation period occurred during 5–9 December (PP1), during 11–17 December (PP2) before restriction, and during December 19 and 26 with restriction.

2.2. PMF Model

The origins of $PM_{2.5}$ were analyzed with the positive matrix factorization (PMF) model of USEPA version 5.0. The model is a widely used receptor model, has high efficiency and convenience without the use of pollution discharge conditions, and allows additional constraints to be added into the factor profiles or factor contributions to reduce result uncertainties [42,43]. Input factors for the model included eight water soluble ions (e.g., Na^+, NH_4^+, K^+, Mg^{2+}, Ca^{2+}, NO_3^-, SO_4^{2-}, and Cl^-), and nine target metal elements (e.g., Al, Fe, Ti, Mn, Cu, Zn, Sb, Pb, and Cr) as well as the $PM_{2.5}$ mass concentration. In this study, five source types were tested in the analysis.

Int. J. Environ. Res. Public Health **2022**, *19*, 6405

4 of 13

2.3. Air Mass Backward Trajectories Cluster Analysis

Backward trajectories of air mass arriving at the sample site (34.76° N, 113.70° E) were calculated for 48 h using the off-line HYSPLIT 4 model. Archived meteorological data with a 1° × 1° latitude–longitude grid and 3 h time interval were used for the trajectory calculations and were provided by the US National Centers for Environmental Prediction Global Data Assimilation System (GDAS) (ftp://arlftp.arlhq.noaa.gov/pub/archives/gdas1, accessed on 5 December 2021). The arrival altitude was set at 500 m above ground level (a.g.l.). The model was run each hour during the whole period focused on in this study.

3. Results and Discussion

3.1. Weather Conditions and Haze Pollution

An extremely severe haze pollution episode occurred between December 19 and 26 after the emergency response measures for heavily polluting weather were implemented on 19 December. The wind speed was usually less than 2 m s^{-1} and the RH was mostly greater than 40% between December 19 and 26, indicating that air movement was stagnant. Under these weather conditions, pollutants were hardly diffused. PM_{10} and $PM_{2.5}$ concentrations started to increase from 43 and 28 μg m^{-3} sharply in the afternoon (13:00–14:00 local time) on 18 December 2019, and the high levels lasted until the morning (10:00–11:00) on December 26 (Figure 2). The maximal mass concentration of PM_{10} and $PM_{2.5}$ reached 332 and 254 μg m^{-3} at night on 25 December, respectively. The wind speed was 1.4 m s^{-1} and the RH was 89%. SIA concentration was 185 μg m^{-3}, accounting for 73% of $PM_{2.5}$ concentration. Under the stable weather conditions, high SIA formation was the major reason for the extremely high aerosol load. The average mass concentrations of PM_{10} and $PM_{2.5}$ during the haze period were 216.86 and 172.63 μg m^{-3}, indicating the extremely high levels of aerosol pollution. The mass concentration ratios of $PM_{2.5}/PM_{10}$ during 19–26 December, i.e., the haze occurrence period (hereafter called HOP) was 0.80, indicating the dominance of $PM_{2.5}$ in the total aerosol mass.
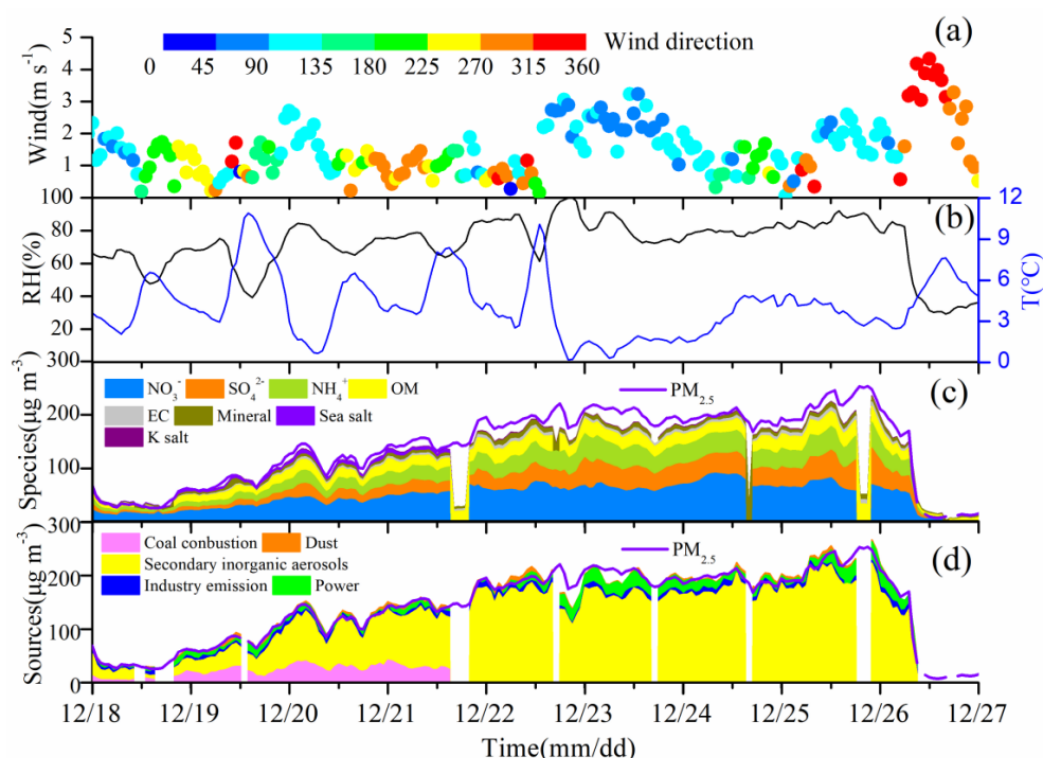

Figure 2. Meteorological conditions (**a,b**), concentration and chemical species of $PM_{2.5}$ (**c**), and contributions from each identified source of $PM_{2.5}$ (**d**) during 18−26 December 2019.

The average concentrations of SO_2, O_3, CO, NO, and NO_2 were 10, 12, 2, 23, and 64 μg m^{-3}, respectively, in the HOP. The SO_2 and NO_2 concentrations were lower than those during a haze episode between January 12 and 23, 2018 in Zhengzhou, but the O_3 concentration was similar [16]. The mass concentration of CO also rose with $PM_{2.5}$. The mass concentrations of SO_2 and O_3 were high in the daytime, with the maximum concentration in the noon or early afternoon, and low in the nighttime on 18–22 December (Figure 3). The trend in SOR followed that of RH quite well; it was high during the night but low during the day and more SO_2 was converted during nighttime [10,11,18]. In comparison, the conversion during daytime was small, and SO_2 concentration was relatively high during the daytime. As O_3 was formed through photochemical reaction, O_3 was high in the daytime [12,14,15]. After a rapid increase of NO_2 concentration in the late afternoon on December 18, NO_2 concentration stayed high in the nighttime and became low in the late afternoon during 18–22 December. It was attributed to NO_2 that was oxidized by hydroxyl radical (OH) and high O_3 to form HNO_3 in the daytime [13,14,16]. This phenomenon was found by other researchers [14,44]. The concentrations of SO_2, O_3, and NO_2 were approximately stable during other periods. SO_2 increased ~6%, NO_2 43%, CO 107.45%, and NO 220.58% from the time before the haze (i.e., before 18 December) to the time of the HOP.
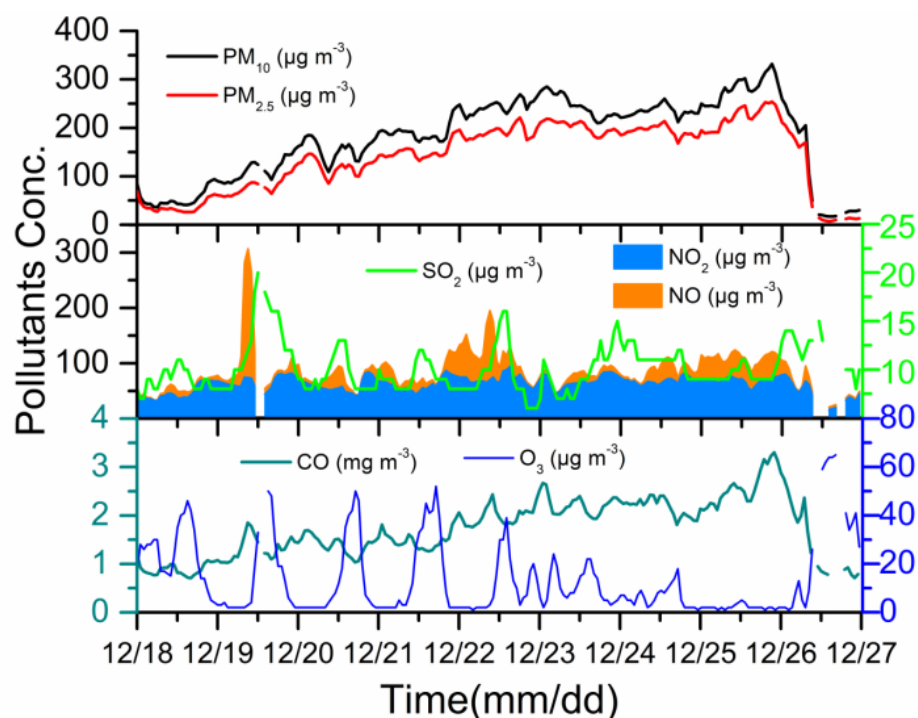

Figure 3. Evolution of particulate matter (PM_{10} and $PM_{2.5}$) and gaseous pollutants (NO, NO_2, SO_2, CO, and O_3) from December 18 to 26.

The increases of different gas pollutants varied with haze development. This phenomenon could be attributed to the differences in the relevant chemical reactions and the responses to emergency response measures. Here we use the concentration of CO as the reference value to investigate the roles of chemical reactions in the variation because CO was produced only from primary emissions and was a very inertial species to the chemical reactions [40,41]. The variability of CO was dominated by emission intensity and atmospheric physical processes (dilution/mix effect). The normalized concentration of $PM_{2.5}$ and precursors by CO can counteract the effect of atmospheric physical processes and represent the contribution of chemical reactions.

With the development of the haze pollution, the ratio of $PM_{2.5}$/CO rapidly increased between the afternoon of 18 December and 22 December, then slightly increased between

Int. J. Environ. Res. Public Health **2022**, *19*, 6405

6 of 13

23 December and the morning of 26 December, and finally largely reduced (Figure S1), reflecting an elevated production rate of secondary species in the HOP. The SO_2/CO and NO_2/CO ratios decreased with haze pollution development, which was consistent with the substantially increasing $PM_{2.5}/CO$ between 19–26 December (Figure S1). This result implies that the air pollution on 19–26 December likely had not been eliminated, although emergency measures had been enacted. A recent study found that, despite emission reductions of 90% across all sectors over Beijing and surrounding provinces, heavily polluted days with daily mean $PM_{2.5}$ higher than 225 $\mu g\ m^{-3}$ may not have been eliminated enough to meet national air quality standards [4].

3.2. Chemical Composition of PM$_{2.5}$ during the HOP

In the HOP, the average concentration of SIAs (including NO_3^-, NH_4^+, and SO_4^{2-}), OM, EC, minerals, sea salt, and K salt were 102.8, 20.3, 4.3, 6.1, 2.2, and 1.1 $\mu g\ m^{-3}$, respectively. SIAs were the major components in the $PM_{2.5}$ and contributed approximately 68%, followed by OM (13%), minerals (4%), EC (3%), sea salt (1%), and K salt (1%) (Figure 2c). Although the mass concentrations of chemical species in $PM_{2.5}$ obviously increased during the HOP, the relative contributions of chemical species to $PM_{2.5}$ varied differently. The contribution of SO_4^{2-} increased by 4.5%, and that of NH_4^+ by 1.0%, whereas the contribution of OM, NO_3^-, sea salt, and mineral cations reduced by 8.95%, 3.94%, 3.88%, and 3.20%. The contribution of NO_3^- and SO_4^{2-} to $PM_{2.5}$ was higher (51%) compared to those in previous studies on $PM_{2.5}$ in Zhengzhou [23,28,45].

RH, T, and O_3 are key factors regulating the oxidation pathways for nitrate and sulfate formation [46–48]. Although SO_2 and NO_2 did not directly result in haze occurrence, approximately 119 $\mu g\ m^{-3}$ of the 173 $\mu g\ m^{-3}$ $PM_{2.5}$ was SIAs, which was related to the two precursor gases during the HOP.

To identify the factors associated with the efficient formation of the SIAs, we compared the formation of NO_3^- and SO_4^{2-} under different levels of their precursor gases, RH, and oxidation ratios. NO_3^- and SO_4^{2-} positively correlated with RH during the HOP (Figure 4a,b). They rapidly increased from 30 $\mu g\ m^{-3}$ to 90 $\mu g\ m^{-3}$ and from 15 $\mu g\ m^{-3}$ to 70 $\mu g\ m^{-3}$, respectively, as the RH increased from 70% to 100%, suggesting NO_3^- and SO_4^{2-} were efficiently produced in moisture air. Regarding the formation of nitrate and sulfate being usually dominated by heterogeneous reactions under high RH (RH > 60%) conditions and by gas-phase reactions at low RH (RH < 30%) conditions [49,50], the efficient production of the two salts in the present case could be attributed to heterogeneous reactions under high RH conditions. High RH favored NO_3^- and SO_4^{2-} formation and subsequently led to the rapid increase of $PM_{2.5}$.

It was found that higher SOR led to a rapid increase of SO_4^{2-} at a given RH, whereas NOR did not. SO_4^{2-} formation was more closely associated with the secondary conversion rate than NO_3^- formation. Rapid increases in NO_3^- were accompanied by large NOR even at low levels of NOx or by low NOR with high NO_x levels (Figure S2). NO_3^- at high NOx levels was produced as efficiently as that of high NOR with low NO_x levels. This result highlights that the NO_3^- production was significantly influenced by both NO_x concentration and the NOR.

As shown in Figure 4c,d, both NOR and SOR were positively correlated with RH. This is consistent with high RH favoring the conversion of aerosol precursors gases (e.g., NO_x and SO_2) to NO_3^- and SO_4^{2-} [1,2,7,9,12]. SOR and NOR were very small (<0.2) when RH was lower than 70% with high O_3 concentration. In contrast, SOR and NOR were dramatically enhanced to 0.8 and 0.5, respectively, when RH increased from 70% to 100% under low O_3. Therefore, the high RH was most likely the major reason for the large SOR and NOR, but low O_3 concentration was not.
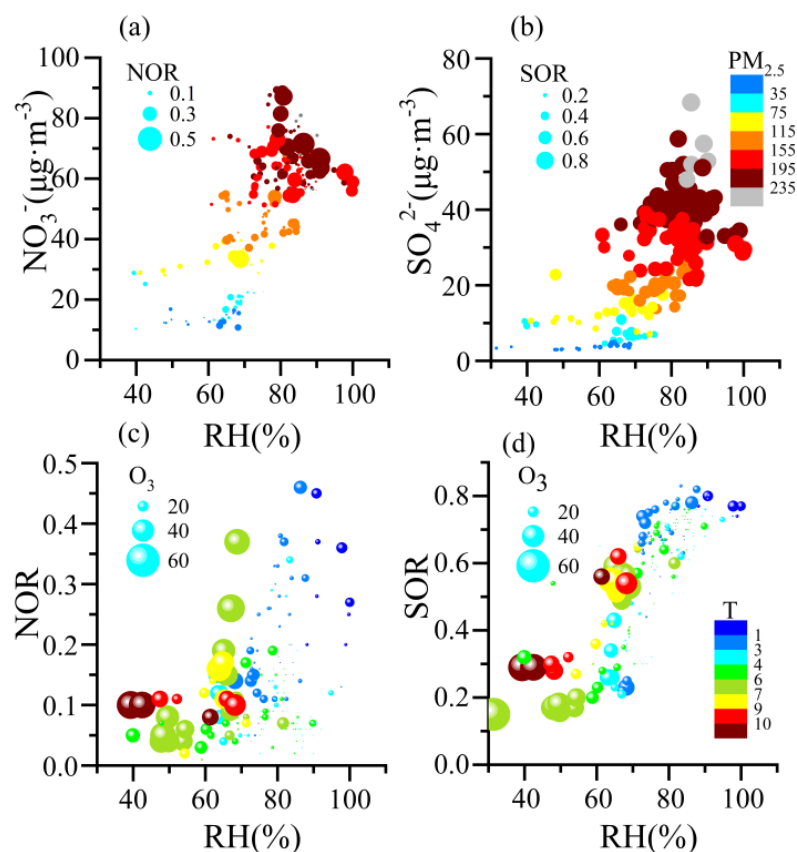
Figure 4. Correlations between RH with NO_3^- (**a**), SO_4^{2-} (**b**), NOR (**c**), and SOR (**d**). Symbols in (**a**,**b**) are scaled by NOR and SOR and colored by $PM_{2.5}$ concentration; Symbols in (**c**,**d**) are scaled by O_3 concentration and colored by temperature (T).

3.3. Inter-Comparison within the Whole Observation Period

3.3.1. Difference in Chemical Composition and Conversions

The haze occurred between 19–26 December 2019. The average concentration of OM in the HOP was 22.10 μg m^{-3}, which was close to that (23.63 μg m^{-3}) during the polluted period between 5–9 December (PP1) and that (21.18 μg m^{-3}) during the polluted period between 11–17 December (PP2) before the restriction. In addition, the average total concentrations of nitrogen compounds (NO_x + NO_3^-: 3.25 μmol m^{-3}) and sulfur compounds (SO_2 + SO_4^{2-}: 0.48 μmol m^{-3}) during the HOP were similar to those during PP1 and PP2 (2.75–3.27 μmol m^{-3} and ~0.38 μmol m^{-3}). These results indicate that nitrogen and sulfur was weakly influenced by the restriction measures. On the contrary, the average concentrations of NO_3^- and SO_4^{2-} in the HOP (57.42 and 30.66 μg m^{-3}) were higher than those during PP1 (37.07 and 18.02 μg m^{-3}) and during PP2 (29.43 and 11.41 μg m^{-3}), although the precursor gas levels were lower during the HOP. NO_3^- and SO_4^{2-} contributed together as much as ~51% of $PM_{2.5}$, which was higher than those in PP1 (~40%) and in PP2 (~39%) before restriction. Therefore, the rapid formations of nitrate and sulfate promoted $PM_{2.5}$ level and caused the severe haze under the restrictions. It was reported that enhanced secondary aerosols might have offset the reduction in primary emissions or decrease in $PM_{2.5}$ in Shanghai, Beijing, and Xi'an [32,43,51,52].

3.3.2. Difference in Source Apportionment and Trajectory Clustering

Coal combustion, industry emission, dust, power, and secondary inorganic aerosols were five $PM_{2.5}$ sources in the PMF analysis (Figure S3). Backward trajectory analysis was then used to investigate the effects of the ranges of source areas influencing the observed $PM_{2.5}$. Three trajectory clusters for each hour in the PP1, PP2, and HOP were acquired via

Int. J. Environ. Res. Public Health **2022**, *19*, 6405

8 of 13

clustering (Figure 5a–c). The proportion of source apportionment of PM$_{2.5}$ corresponding to each trajectory cluster are also presented in Figure 5d–f. The source regions of air mass and source apportionment varied largely in the PP1, PP2, and HOP.
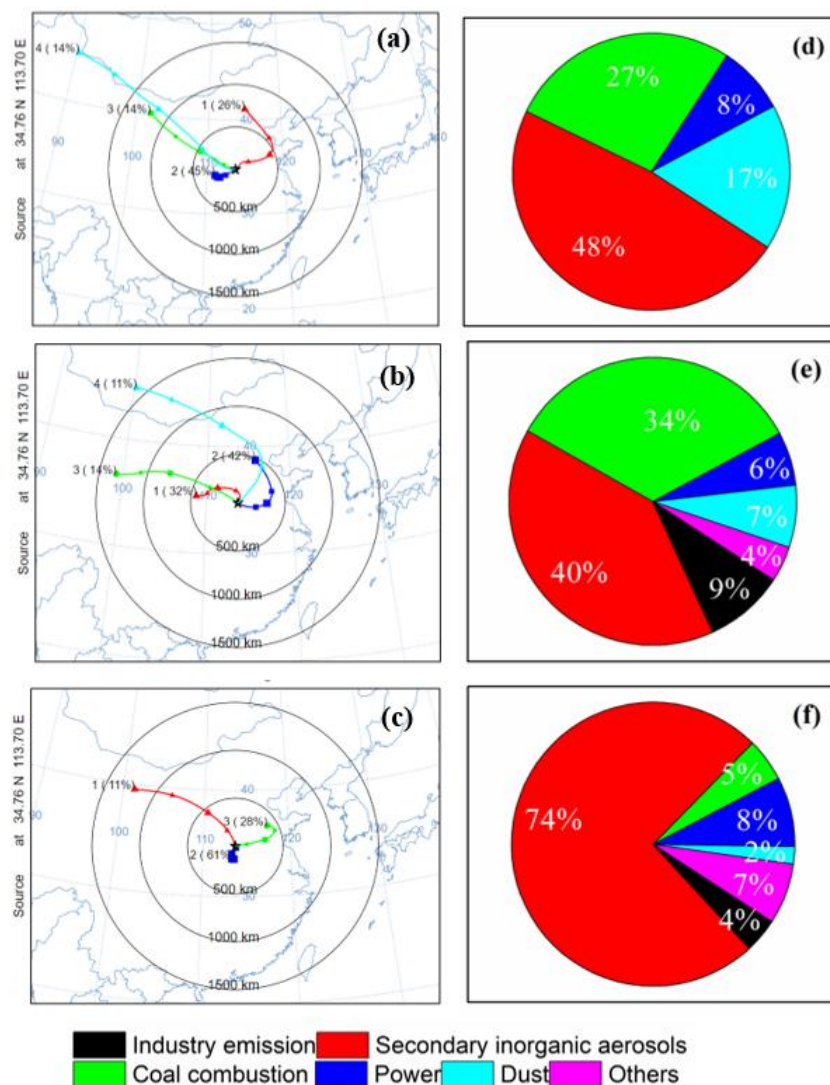

Figure 5. Examples of cluster mean 48 h backward air trajectories and source contribution fractions to PM$_{2.5}$ in PP1 (**a**,**d**), PP2 (**b**,**e**), and HOP (**c**,**f**).

In PP1 before the restriction, 45% of air parcels were from southwestern areas about 300 km away from Zhengzhou (such as Xi'an, Sanmenxia, and Luoyang), where there are few heavy and light industries. The movement of the air mass was slow with average speed 1.7 m s^{-1}. About 14% of air parcels came from northern and northwester areas about 2000 km and 1200 km away from the city, where there are few industrial activities. These air masses moved very quickly and passed arid and semi-arid areas. The contribution of mineral dust to PM$_{2.5}$ was large (17%) in comparison to the other two periods. In PP2 before the restriction, 42% of air parcels came from northeastern areas about 500 km away from the city, where there are various heavy and light industries. About 32% of air parcels came from western areas 500 km away from Zhengzhou (such as Xi'an, Yuncheng, and Jiaozuo), which are coal-rich cities. The moving speed of air masses was about 2.9 m s^{-1}. The contribution of coal combustion to PM$_{2.5}$ in PP2 was ~34%, indicating that the air mass from those areas was heavily polluted.

In the HOP, a large proportion of air parcels (52%) moved stagnantly around the southern area about 200 km south at the speed of 1.2 m s^{-1}, suggesting that pollutants

from the local areas dominated the air pollution (Figure 5c). The PM$_{2.5}$ concentration was approximately four-fold higher than that before the haze formation. Furthermore, both the mass and contribution of coal combustion to PM$_{2.5}$ in this cluster decreased in comparison to PP1 and PP2 (Figure 5), which was due to the restriction. However, the contribution of SIAs (secondary inorganic aerosols) to PM$_{2.5}$ was the highest (~75%) in comparison to those in PP1 and PP2, indicating the formation of SIAs was the major reason for the haze occurrence.

3.3.3. Significance of SIA Formation in HOP

The oxidation pathways for nitrate and sulfate formation were influenced by RH, temperature, and O$_3$ [8,46–50]. O$_3$ decreased during the HOP and high NOR and SOR were accompanied by low O$_3$ (Figure 4). O$_3$ was unlikely to have been the major oxidant for the large SIA formation. The RH in the HOP was 78.12%, higher than the 67.86% in PP1 and 51.37% in PP2. The high RH in the HOP was caused by frequent artificial spreading of water vapor in the urban air, a special measure of the Zhengzhou local government to reduce air pollution.

NOR and SOR increased with RH, which is consistent with the fact that high RH favors the conversion of the precursor gases to nitrate and sulfate [1,2,7,9,12]. NOR and SOR were much higher in the HOP than those in PP1 and PP2, when the RH was larger than 70%. (Figure 6). Moreover, the corresponding NO$_3^-$ and SO$_4^{2-}$ showed obvious rapid increases under RH > 70% than those under RH < 70% (Figure 4). These results indicate high RH (>70%), related to water-vapor spreading during the HOP, which led to the enlargement of the conversion rates of NO$_3^-$ and SO$_4^{2-}$. Zang et al. (2019) found that sulfate (SO$_4^{2-}$) and nitrate (NO$_3^-$) were enhanced by approximately 2-fold and 1.5-fold, respectively, under wet conditions [50]. The results indicated that high RH favors the formation of sulfate and nitrate, implying that low RH might help to reduce PM$_{2.5}$ pollution.
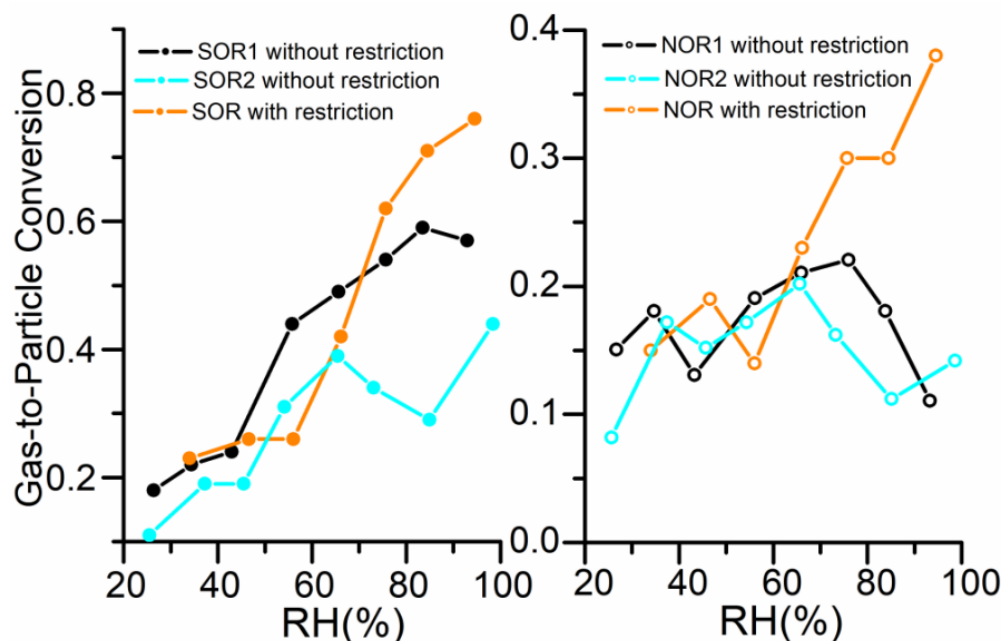

Figure 6. Correlations between SOR, NOR, and RH, and SOR and RH with and without the restriction.

If NOR and SOR in the restriction period were not 0.3 and 0.64, but instead were similar to those (0.21 and 0.5) before the restriction (Table 2), the concentration of NO$_3^-$ would have been smaller by 19.04 μg m^{-3} and that of SO$_4^{2-}$ by 15.32 μg m^{-3}. NH$_4^+$ could also have been reduced by 14.65 μg m^{-3}. PM$_{2.5}$ levels would have been lower than at least 108.18 μg m^{-3} during the restriction period. These results support the idea that high gas-to-particle conversions in the moisture air under low pollutant emission enhanced

NO_3^- and SO_4^{2-} formations, hindering $PM_{2.5}$ reduction, and consequently leading to the severe haze occurrence [26,51,52].

Table 2. Average concentration and deviation (in μg m^{-3}) of $PM_{2.5}$, $PM_{2.5}$ contents of ions, OM, EC, and precursor gases of SO_2 and NO_x; average rates of gas-to-particle conversion (NOR, SOR); and RH (in %) in the three periods of PP1, PP2, and HOP.

	PP1 before Restriction	**PP2 before Restriction**	**HOP with Restriction**
$PM_{2.5}$	136.35 ± 37.53	104.162 ± 2.17	172.63 ± 43.10
NO_3^-	37.07 ± 10.10	29.43 ± 7.08	57.42 ± 14.98
SO_4^{2-}	18.02 ± 5.39	11.41 ± 4.54	30.66 ± 11.80
NH_4^+	20.36 ± 5.68	14.67 ± 3.36	30.88 ± 8.93
OM	23.63 ± 8.43	21.18 ± 4.96	22.10 ± 5.07
EC	3.27 ± 1.29	3.13 ± 1.02	4.83 ± 1.49
NO_x	122.59 ± 59.43	104.48 ± 44.42	107.12 ± 52.64
SO_2	12.27 ± 6.29	16.23 ± 5.00	10.23 ± 2.43
O_3	16.37 ± 22.35	15.81 ± 19.55	9.81 ± 11.62
NOR	0.21 ± 0.08	0.19 ± 0.07	0.30 ± 0.08
SOR	0.50 ± 0.13	0.33 ± 0.14	0.64 ± 0.12
RH	67.86 ± 17.40	51.37 ± 9.99	78.12 ± 10.05

3.3.4. Inter-Comparisons of the Responses of Secondary Aerosol Formations to Emissions Reductions

A severe haze pollution occurred in Zhengzhou between 19–26 December 2019, though the emergency response measure caused decreases in $PM_{2.5}$ mass from coal combustion by 60–66% and dust by 24–79% compared to those before the restriction. Many studies have reported that the $PM_{2.5}$ level in China decreased by 29.79% from 2016 to 2020, due to reductions on the emissions of NO_x and SO_2, but haze pollution still occurs in northern China in winter [10,20,23,53]. The enhancement of secondary pollution was the major reason for the haze pollution [54,55]. Sulfate and nitrate have changed little in the past decade over the eastern United States, accounting for half of the $PM_{2.5}$ mass, despite a substantial reduction in precursors emissions [56]. SO_4^{2-} was reduced significantly by 73.3%; however, NO_3^- was reduced relatively less significantly by 29.1%, although emissions of SO_2 and HNO_3 in the United States and Canada were significantly reduced by 87.6% and 65.8% from 1990 to 2015 [57].

Results of the present study showed that high SIA concentration formation caused severe haze despite the implementation of emergency response measures to restrict the anthropogenic pollutants. Simulations revealed that limitations of the availability of oxidants relax at lower precursor concentrations, producing particulate matter more efficiently, and weakening the effectiveness of emission reductions over the eastern United States [56]. Due to a notable change in regional chemistry, SOR and NOR increased by more than 50% during the cold season causing the nonlinear relationships between SO_4^{2-}, NO_3^-, and their precursors in the United States and Canada [57]. These results suggest that substantial improvements in air quality need larger emission reductions in China, the United States, and Canada.

4. Conclusions

In this study, chemical species, positive matrix factorization (PMF), and trajectory clustering were applied to characterize the chemical conversion and explore potential origins of $PM_{2.5}$ to investigate the reasons for the severe haze occurrence in Zhengzhou during 19–26 December, after the emergency response measures were implemented to suppress air pollution in the city.

During the HOP, the average concentration of $PM_{2.5}$ was 172.63 μg m^{-3}. The average concentrations of SO_2 and NO_2 were 10.23 μg m^{-3} and 66.76 μg m^{-3}, which were lower than those in PP1 and PP2. NOR and SOR increased quickly with RH during the HOP when RH was >70%. Large amounts of sulfate (31 μg m^{-3}) and nitrate (57 μg m^{-3}) were produced

under the high RH and contributed to 51% of $PM_{2.5}$ during the HOP. These results indicate that the severe haze was mainly caused by sulfate and nitrate formation via efficient gas-to-particle conversions in moisture air under the restriction of air pollutant emissions. The five $PM_{2.5}$ sources were secondary inorganic aerosols, industry emissions, dust, power, and coal combustion. The contribution of secondary inorganic aerosols to the $PM_{2.5}$ in the HOP was highest (74%). In addition, most air mass came from surrounding areas in the south and moved slowly to the city during the HOP, suggesting the dominance of pollutants from local areas in the $PM_{2.5}$ elevation. In conclusion, high gas-to-particle conversions in the moisture air resulted in efficient formation of secondary inorganic aerosols, and thereby caused the severe haze in Zhengzhou, despite implementation of emergency response measures to restrict the anthropogenic pollutants. The result implies that lowering RH might help to decay and even suppress the formation of SIAs. Therefore, the activities of watering, spraying, and wet sweeping should be limited in order to reduce haze pollution in the city, since these activities must have caused RH growth in the urban air.

Supplementary Materials: The following supporting information can be downloaded at: https://www.mdpi.com/article/10.3390/ijerph19116405/s1, Figure S1: Time series of $PM_{2.5}$ and gaseous pollutants (NO, NO_2, SO_2, CO and O_3) in the three periods. Figure S2: Correlations between NO_3^- and NO_x, SO_4^{2-} and RH. Symbols in (a) are scaled by NOR, and colored by $PM_{2.5}$ concentration; Symbols in (b) are scaled by SOR concentration, and colored by SO_2. Figure S3: Profiles of four sources profiles (bars) resolved from the PMF model (in units of $\mu g\ \mu g^{-1}$) and contribution percentages (black dots) from each source factor.

Author Contributions: Conceptualization, Q.M.; methodology, W.W.; software, R.Z. and J.Z.; validation, D.L. and W.L.; formal analysis, Q.M.; data curation, Q.M.; writing—original draft preparation, Q.M.; writing—review and editing, D.Z. and Y.P. All authors have read and agreed to the published version of the manuscript.

Data Availability Statement: Not applicable.

Conflicts of Interest: The authors declared that they have no conflicts of interest to this work. We declare that we do not have any commercial or associative interest that represents a conflict of interest in connection with the work submitted.

References

1. Cheng, Y.F.; Zheng, G.J.; Wei, C.; Mu, Q.; Zheng, B.; Wang, Z.B.; Gao, M.; Zhang, Q.; He, K.B.; Carmichael, G.; et al. Reactive nitrogen chemistry in aerosol water as a source of sulfate during haze events in China. *Sci. Adv.* **2016**, *2*, 11. [CrossRef] [PubMed]
2. Ma, Q.X.; Wu, Y.F.; Zhang, D.Z.; Wang, X.J.; Xia, Y.J.; Liu, X.Y.; Tian, P.; Han, Z.W.; Xia, X.A.; Wang, Y.; et al. Roles of regional transport and heterogeneous reactions in the $PM_{2.5}$ increase during winter haze episodes in Beijing. *Sci. Total Environ.* **2017**, *599–600*, 246–253. [CrossRef] [PubMed]
3. Song, X.Y.; Jia, J.; Wu, F.; Niu, H.Y.; Ma, Q.X.; Guo, B.; Shao, L.Y.; Zhang, D.Z. Local emissions and secondary pollutants cause severe $PM_{2.5}$ elevation in urban air at the south edge of the North China Plain: Results from winter haze of 2017-2018 at a mega city. *Sci. Total Environ.* **2022**, *802*, 149630. [CrossRef] [PubMed]
4. Ansari, T.; Wild, O.; Ryan, E.; Chen, Y.; Li, J.; Wang, Z. Temporally resolved sectoral and regional contributions to air pollution in Beijing: Informing short-term emission controls. *Atmos. Chem. Phys.* **2021**, *21*, 4471–4485. [CrossRef]
5. Yan, Y.; Zhou, Y.; Kong, S.; Lin, J.; Wu, J.; Zheng, H.; Zhang, Z.; Song, A.; Bai, Y.; Ling, Z.; et al. Effectiveness of emission control in reducing $PM_{2.5}$ pollution in central China during winter haze episodes under various potential synoptic controls. *Atmos. Chem. Phys.* **2021**, *21*, 3143–3162. [CrossRef]
6. Zhong, Q.; Tao, S.; Ma, J.; Liu, J.; Shen, H.; Shen, G.; Guan, D.; Yun, X.; Meng, W.; Yu, X.; et al. $PM_{2.5}$ reductions in Chinese cities from 2013 to 2019 remain significant despite the inflating effects of meteorological conditions. *One Earth* **2021**, *4*, 448–458. [CrossRef]
7. Peng, J.F.; Hu, M.; Shang, D.J. Explosive Secondary Aerosol Formation during Severe Haze in the North China Plain. *Environ. Sci. Technol.* **2021**, *55*, 2189–2207. [CrossRef]
8. Ma, Q.X.; Wu, Y.F.; Fu, S.L.; Zhang, D.Z.; Han, Z.W.; Zhang, R.J. Pollution severity-dependent aerosol light scattering enhanced by inorganic species formation in Beijing haze. *Sci. Total Environ.* **2020**, *719*, 137545. [CrossRef]

Int. J. Environ. Res. Public Health **2022**, *19*, 6405

12 of 13

9. Wang, G.; Zhang, R.; Gomez, M.E.; Yang, L.; Zamora, M.L.; Hu, M.; Lin, Y.; Peng, J.; Guo, S.; Meng, J.; et al. Persistent sulfate formation from London fog to Chinese haze. *Proc. Natl. Acad. Sci. USA* **2016**, *113*, 13630–13635. [CrossRef] [PubMed]

10. Meng, F.; Zhang, Y.; Kang, J.; Heal, M.R.; Reis, S.; Wang, M.; Liu, L.; Wang, K.; Yu, S.; Li, P.; et al. Trends in secondary inorganic aerosol pollution in China and its responses to emission controls of precursors in wintertime. *Atmos. Chem. Phys.* **2022**, *22*, 6291–6308. [CrossRef]

11. Liu, L.; Zhang, J.; Du, R.G.; Teng, X.M.; Hu, R.; Yuan, Q.; Tang, S.S.; Ren, C.H.; Huang, X.; Xu, L.; et al. Chemistry of Atmospheric Fine Particles during the COVID-19 Pandemic in a Megacity of Eastern China. *Geophys. Res. Lett.* **2021**, *48*, e2020GL091611. [CrossRef]

12. Gen, M.S.; Zhang, R.F.; Huang, D.D.; Li, Y.J.; Chan, C.K. Heterogeneous Oxidation of SO_2 in Sulfate Production during Nitrate Photolysis at 300 nm: Effect of pH, Relative Humidity, Irradiation Intensity, and the Presence of Organic Compounds. *Environ. Sci. Technol.* **2019**, *53*, 8757–8766. [CrossRef]

13. Lin, Y.C.; Zhang, Y.L.; Fan, M.Y.; Bao, M.Y. Heterogeneous formation of particulate nitrate under ammonium-rich regimes during the high-$PM_{2.5}$ events in Nanjing, China. *Atmos. Chem. Phys.* **2020**, *20*, 3999–4011. [CrossRef]

14. Fu, X.; Wang, T.; Gao, J.; Wang, P.; Liu, Y.; Wang, S.; Zhao, B.; Xue, L. Persistent heavy winter nitrate pollution driven by increased photochemical oxidants in northern China. *Environ. Sci. Technol.* **2020**, *54*, 3881–3889. [CrossRef]

15. Wang, J.F.; Li, J.Y.; Ye, J.H.; Zhao, Y.; Wu, J.Z.; Hu, J.L.; Liu, D.T.; Nie, D.Y.; Shen, F.Z.; Huang, X.P.; et al. Fast sulfate formation from oxidation of SO_2 by NO_2 and HONO observed in Beijing haze. *Nat. Commun.* **2020**, *11*, 2844. [CrossRef]

16. Ye, S.Q.; Ma, T.; Duan, F.K.; Li, H.; He, K.B.; Xia, J.; Yang, S.; Zhu, L.D.; Ma, Y.L.; Huang, T.; et al. Characteristics and formation mechanisms of winter haze in Changzhou, a highly polluted industrial city in the Yangtze River Delta, China. *Environ. Pollut.* **2019**, *253*, 377–383. [CrossRef]

17. George, C.; Ammann, M.; D'Anna, B.; Donaldson, D.J.; Nizkorodov, S.A. Heterogeneous photochemistry in the atmosphere. *Chem. Rev.* **2015**, *115*, 4218–4258. [CrossRef]

18. An, Z.; Huang, R.; Zhang, R.; Tie, X.; Li, G.; Cao, J.; Zhou, W.; Shi, Z.; Han, Y.; Gu, Z.; et al. Severe haze in northern China: A synergy of anthropogenic emissions and atmospheric processes. *Proc. Natl. Acad. Sci. USA* **2019**, *116*, 8657–8666. [CrossRef]

19. Xia, Y.J.; Wu, Y.F.; Huang, R.J.; Xia, X.A.; Tang, J.; Wang, M.; Li, J.W.; Wang, C.Y.; Zhou, C.; Zhang, R.J. Variation in black carbon concentration and aerosol optical properties in Beijing: Role of emission control and meteorological transport variability. *Chemosphere* **2020**, *254*, 126849. [CrossRef]

20. Li, W.; Shao, L.; Wang, W.; Li, H.; Wang, X.; Li, Y.; Li, W.; Jones, T.; Zhang, D. Air quality improvement in response to intensified control strategies in Beijing during 2013–2019. *Sci. Total Environ.* **2020**, *744*, 140776. [CrossRef]

21. Li, X.; Zhao, B.; Zhou, W.; Shi, H.; Yin, R.; Cai, R.; Yang, D.; Dallenbach, K.; Deng, C.; Fu, Y.; et al. Responses of gaseous sulfuric acid and particulate sulfate to reduced SO_2 concentration: A perspective from long–term measurements in Beijing. *Sci. Total Environ.* **2020**, *721*, 137700. [CrossRef]

22. Zhang, Z.; Guan, H.; Luo, L.; Zheng, N.; Xiao, H. Response of fine aerosol nitrate chemistry to Clean Air Action in winter Beijing: Insights from the oxygen isotope signatures. *Sci. Total Environ.* **2020**, *746*, 141210. [CrossRef]

23. Zhang, W.; Wang, H.; Zhang, X.; Peng, Y.; Zhong, J.; Wang, Y.; Zhao, Y. Evaluating the contributions of changed meteorological conditions and emission to substantial reductions of $PM_{2.5}$ concentration from winter 2016 to 2017 in Central and Eastern China. *Sci. Total Environ.* **2020**, *716*, 136892. [CrossRef]

24. Ghosal, R.; Saha, E. Impact of the COVID-19 induced lockdown measures on $PM_{2.5}$ concentration in USA. *Atmos. Environ.* **2021**, *254*, 118388. [CrossRef]

25. Jeong, C.; Yousif, M.; Evans, G. Impact of the COVID-19 lockdown on the chemical composition and sources of urban $PM_{2.5}$. *Environ. Pollut.* **2022**, *292*, 118417. [CrossRef]

26. Du, H.Y.; Li, J.; Wang, Z.F.; Yang, W.Y.; Chen, X.S.; Wei, Y. Sources of $PM_{2.5}$ and its responses to emission reduction strategies in the Central Plains Economic Region in China: Implications for the impacts of COVID-19. *Environ. Pollut.* **2021**, *288*, 117783. [CrossRef]

27. Liu, S.; Hua, S.; Wang, K.; Qiu, P.; Liu, H.; Wu, B.; Shao, P.; Liu, X.; Wu, Y.; Xue, Y.; et al. Spatial-temporal variation characteristics of air pollution in Henan of China: Localized emission inventory, WRF/Chem simulations and potential source contribution analysis. *Sci. Total Environ.* **2018**, *624*, 396–406. [CrossRef]

28. Yang, L.; Ren, Q.; Ge, S.J.; Jiao, Z.Q.; Zhan, W.H.; Hou, R.X.; Ruan, X.L.; Pan, Y.F.; Wang, Y.Y. Metal(loid)s Spatial Distribution, Accumulation, and Potential Health Risk Assessment in Soil-Wheat Systems near a Pb/Zn Smelter in Henan Province, Central China. *Int. J. Environ. Res. Public Health* **2022**, *19*, 2527. [CrossRef]

29. Yang, W.Y.; Li, J.; Wang, Z.F.; Wang, L.L.; Dao, X.; Zhu, L.L.; Pan, X.L.; Li, Y.Y.; Sun, Y.L.; Ma, S.L.; et al. Source apportionment of $PM_{2.5}$ in the most polluted Central Plains Economic Region in China: Implications for joint prevention and control of atmospheric pollution. *J. Clean. Prod.* **2021**, *283*, 124557. [CrossRef]

30. Wang, H.; Li, J.H.; Peng, Y.; Zhang, M.; Che, H.Z.; Zhang, X.Y. The impacts of the meteorology features on $PM_{2.5}$ levels during a severe haze episode in central-east China. *Atmos. Environ.* **2019**, *197*, 177–189. [CrossRef]

31. Zhengzhou Municipal People's Government. Available online: http://public.zhengzhou.gov.cn/10K/3525671.jhtml:2019-12-18 (accessed on 12 December 2019).

32. Chen, H.; Huo, J.; Fu, Q.; Duan, Y.; Xiao, H.; Chen, J. Impact of quarantine measures on chemical compositions of $PM_{2.5}$ during the COVID-19 epidemic in Shanghai, China. *Sci. Total Environ.* **2020**, *743*, 140758. [CrossRef] [PubMed]

Int. J. Environ. Res. Public Health **2022**, *19*, 6405

13 of 13

33. Stieger, B.; Spindler, G.; Fahlbusch, B.; Müller, K.; Grüner, A.; Poulain, L.; Thöni, L.; Seitler, E.; Wallasch, M.; Herrmann, H. Measurements of PM_{10} ions and trace gases with the online system MARGA at the research station Melpitz in Germany—A five-year study. *J. Atmos. Chem.* **2018**, *75*, 33–70. [CrossRef]

34. Yang, Y.R.; Liu, X.G.; Qu, Y.; Wang, J.L.; An, J.L.; Zhang, Y.H.; Zhang, F. Formation mechanism of continuous extreme haze episodes in the megacity Beijing, China, in January 2013. *Atmos. Res.* **2015**, *155*, 192–203. [CrossRef]

35. Zhang, R.J.; Jing, J.; Tao, J.; Hsu, S.-C.; Wang, G.; Cao, J.; Lee, C.S.L.; Zhu, L.; Chen, Z.; Zhao, Y.; et al. Chemical characterization and source apportionment of $PM_{2.5}$ in Beijing: Seasonal perspective. *Atmos. Chem. Phys.* **2013**, *13*, 7053–7074. [CrossRef]

36. Malm, W.C.; Sisler, J.F.; Huffman, D.; Eldred, R.A.; Cahill, T.A. Spatial and seasonal trends in particle concentration and optical extinction in the United States. *J. Geophys. Res.* **1994**, *99*, 1347–1370. [CrossRef]

37. Chow, J.C.; Watson, J.G.; Fujita, E.M.; Lu, Z.; Lawson, D.R. Temporal and spatial variation of $PM_{2.5}$ and PM_{10} aerosol in the Southern California air quality study. *Atmos. Environ.* **1994**, *28*, 2061–2080. [CrossRef]

38. Hsu, S.C.; Liu, S.C.; Tsai, F.; Engling, G.; Lin, I.I.; Chou, C.K.C.; Kao, S.J.; Lung, S.C.C.; Chan, C.Y.; Lin, S.C.; et al. High wintertime particulate matter pollution over an offshore island (Kinmen) off southeastern China: An overview. *J. Geophys. Res.* **2010**, *115*, D17309. [CrossRef]

39. Pósfai, M.; Gelencsér, A.; Simonics, R.; Arató, K.; Li, J.; Hobbs, P.V.; Buseck, P.R. Atmospheric tar balls: Particles from biomass and biofuel burning. *J. Geophys. Res.* **2004**, *109*, D06213. [CrossRef]

40. Han, T.; Liu, X.G.; Zhang, Y.H.; Qu, Y.; Zeng, L.M.; Hu, M.; Zhu, T. Role of secondary aerosols in haze formation in summer in the Megacity Beijing. *J. Environ. Sci.* **2015**, *31*, 51–60. [CrossRef]

41. Zhang, Q.; Quan, J.N.; Tie, X.X.; Li, X.; Liu, Q.; Gao, Y.; Zhao, D.L. Effects of meteorology and secondary particle formation on visibility during heavy haze events in Beijing, China. *Sci. Total Environ.* **2015**, *502*, 578–584. [CrossRef]

42. Tian, Y.; Zhang, Y.; Liang, Y.; Niu, Z.; Xue, Q.; Feng, Y. $PM_{2.5}$ source apportionment during severe haze episodes in a Chinese megacity based on a 5-month period by using hourly species measurements: Explore how to better conduct PMF during haze episodes. *Atmos. Environ.* **2020**, *224*, 117364. [CrossRef]

43. Tian, J.; Wang, Q.; Zhang, Y.; Yan, M.; Liu, H.; Zhang, N.; Ran, W.; Cao, J. Impacts of primary emissions and secondary aerosol formation on air pollution in an urban area of China during the COVID-19 lockdown. *Environ. Int.* **2021**, *150*, 106426. [CrossRef]

44. Zhang, D.; He, B.; Yuan, M.; Yu, S.; Yin, S.; Zhang, R. Characteristics, sources and health risks assessment of VOCs in Zhengzhou, China during haze pollution season. *J. Environ. Sci.* **2021**, *108*, 44–57. [CrossRef]

45. Wang, S.B.; Wang, L.L.; Wang, N.; Ma, S.L.; Su, F.C.; Zhang, R.Q. Formation of droplet-mode secondary inorganic aerosol dominated the increased PM2.5 during both local and transport haze episodes in Zhengzhou, China. *Chemosphere* **2021**, *269*, 128744. [CrossRef]

46. Fang, Y.; Ye, C.; Wang, J.; Wu, Y.; Hu, M.; Lin, W.; Xu, F.; Zhu, T. Relative humidity and O_3 concentration as two prerequisites for sulfate formation. *Atmos. Chem. Phys.* **2019**, *19*, 12295–12307. [CrossRef]

47. Liu, P.F.; Ye, C.; Xue, C.Y.; Zhang, C.L.; Mu, Y.J.; Sun, X. Formation mechanisms of atmospheric nitrate and sulfate during the winter haze pollution periods in Beijing: Gas–phase, heterogeneous and aqueous–phase chemistry. *Atmos. Chem. Phys.* **2020**, *20*, 4153–4165. [CrossRef]

48. Liu, T.; Clegg, S.L.; Abbatt, J.P.D. Fast oxidation of sulfur dioxide by hydrogen peroxide in deliquesced aerosol particles. *PNAS* **2020**, *117*, 1354–1359. [CrossRef]

49. Li, G.; Bei, N.; Cao, J.; Huang, R.; Wu, J.; Feng, T.; Wang, Y.; Liu, S.; Zhang, Q.; Tie, X.; et al. A possible pathway for rapid growth of sulfate during haze days in China. *Atmos. Chem. Phys.* **2017**, *17*, 3301–3316. [CrossRef]

50. Zang, L.; Wang, Z.; Zhu, B.; Zhang, Y. Roles of Relative Humidity in Aerosol Pollution Aggravation over Central China during Wintertime. *Int. J. Environ. Res. Public Health* **2019**, *16*, 4422. [CrossRef]

51. Chang, Y.; Huang, R.; Ge, X.; Huang, X.; Hu, J.; Duan, Y.; Zou, Z.; Liu, X.; Lehmann, M.F. Puzzling haze events in China during the coronavirus (COVID-19) shutdown. *Geophys. Res. Lett.* **2020**, *47*, e2020GL088533. [CrossRef]

52. Duan, J.; Huang, R.J.; Chang, Y.H.; Zhong, H.B.; Gu, Y.F.; Lin, C.S.; Hoffmann, T.; O'Dowd, C. Measurement report of the change of $PM_{2.5}$ composition during the COVID-19 lockdown in urban Xi'an: Enhanced secondary formation and oxidation. *Sci. Total Environ.* **2021**, *791*, 148126. [CrossRef]

53. Ministry of Ecology and Environment of the People's Republic of China (MEE), China Environmental State Bulletin 2020. 2020. Available online: https://www.mee.gov.cn/hjzl/sthjzk/zghjzkgb/ (accessed on 20 March 2021). (In Chinese)

54. Ye, Z.L.; Li, J.; Pan, Y.P.; Wang, Z.F.; Guo, X.R.; Cheng, L.; Tang, X.; Zhu, J.; Kong, L.; Song, Y.; et al. Synergistic effect of reductions in multiple gaseous precursors on secondary inorganic aerosols in winter under a meteorology-based redistributed daily NH3 emission inventory within the Beijing-Tianjin-Hebei region, China. *Sci. Total Environ.* **2022**, *821*, 153383. [CrossRef]

55. Lu, M.M.; Tang, X.; Feng, Y.C.; Wang, Z.F.; Chen, X.S.; Kong, L.; Ji, D.S.; Liu, Z.R.; Liu, K.X.; Wu, H.J.; et al. Nonlinear response of SIA to emission changes and chemical processes over eastern and central China during a heavy haze month. *Sci. Total Environ.* **2021**, *788*, 147747. [CrossRef]

56. Shaha, V.; Jaeglé, L.; Thorntona, J.A.; Lopez-Hilfikera, F.D.; Lee, B.H.; Schroder, J.C.; Campuzano-Jost, P.; Green, J.R.; Fiddler, M.N.; Bililigng, S.; et al. Chemical feedbacks weaken the wintertime response of particulate sulfate and nitrate to emissions reductions over the eastern United States. *Proc. Natl. Acad. Sci. USA* **2018**, *115*, 8110–8115. [CrossRef]

57. Feng, J.; Chan, E.; Vet, R. Air quality in the eastern United States and Eastern Canada for 1990–2015: 25 years of change in response to emission reductions of SO_2 and NO_x in the region. *Atmos. Chem. Phys.* **2020**, *20*, 3107–3134. [CrossRef]